

Geometrical interpretation of dynamical phase transitions in boundary-driven systems

Ohad Shpielberg*

Laboratoire de Physique Théorique de l'École Normale Supérieure de Paris, CNRS, ENS & PSL Research University, UPMC & Sorbonne Universités, 75005 Paris, France

(Received 26 June 2017; revised manuscript received 26 October 2017; published 5 December 2017)

Dynamical phase transitions are defined as nonanalytic points of the large deviation function of current fluctuations. We show that for boundary-driven systems, many dynamical phase transitions can be identified using the geometrical structure of an effective potential of a Hamiltonian, recovered from the macroscopic fluctuation theory description. Using this method we identify new dynamical phase transitions that could not be recovered using existing perturbative methods. Moreover, using the Hamiltonian picture, an experimental scheme is suggested to demonstrate an analog of dynamical phase transitions in linear, rather than exponential, time.

DOI: [10.1103/PhysRevE.96.062108](https://doi.org/10.1103/PhysRevE.96.062108)**I. INTRODUCTION**

The study of phase transitions spans across all branches of physics [1–4]. Thermodynamic phase transitions in equilibrium systems have been studied extensively [5,6]. However, for systems driven out of equilibrium, even simple ideas valid in equilibrium seem to be violated [7]. As a prominent example, we note the Peierls argument: There are no phase transitions in equilibrium $1d$ systems with short-range interactions [6]. This argument breaks down for out-of-equilibrium systems [8–15]. While out-of-equilibrium systems allow for a richer set of effects, a theory comparable to statistical mechanics is lacking.

A major advancement in the understanding of out-of-equilibrium systems is the recent formulation of the macroscopic fluctuation theory (MFT) [16,17]. The MFT offers a hydrodynamic description of steady-state fluctuations in diffusive systems. It was used to characterize steady-state density correlations [18,19], identify fluctuation-induced forces [20], find Clausius inequalities [21], follow the statistics of single-file diffusion [22], and many more [23–29]. With the help of the MFT, it is conceivable that a classification of phase transitions in out-of-equilibrium diffusive systems can be pursued.

In this paper, we focus on current fluctuations in boundary-driven diffusive systems within the framework of the MFT. The study of current fluctuations deals with finding the probability $P_t(Q)$ to observe an atypical charge transfer Q at the long time limit t [30]. Here we restrict the discussion to $1d$ systems only. We assume throughout the text that a large deviation principle applies, namely

$$P_t(Q) \sim \exp[-t \Phi(J = Q/t)], \quad (1)$$

where $\Phi(J)$ is the large deviation function (LDF) of J , the mean current in the system. Obtaining an exact expression for Φ is not a trivial task both analytically [26,31–37] and numerically [38–40]. In boundary-driven diffusive systems, the MFT allows us to write the LDF formally. Finding $\Phi(J)$ reduces to finding the optimal fluctuation of the density profile responsible for the atypical current. Finding this optimal fluctuation is inherently hard. In Ref. [41], it was suggested

that the optimal fluctuation is time-independent (except for a negligible transient time). This conjecture, known as the additivity principle (AP), was shown to be exact for several boundary driven systems [41–44] and is believed to be always valid for currents sufficiently close to the steady state current. In fact, a violation of the AP was found only recently for boundary driven systems [44,45]. Obtaining the large deviation function under the AP assumption boils down to solving boundary valued non-linear differential equations. This allows for the possibility of multiple solutions as was demonstrated in Refs. [46,47]. Multiple optimal solutions may lead to nonanalytic points in the large deviation function [12,46,48]. Transitions between optimal solutions as a function of J (AP violations included) go under the name of dynamical phase transitions (DPT). It is usually hard to find analytically all possible solutions. Moreover, it is appealing to be able to predict the occurrence of DPTs from simple arguments. This goal is pursued here using a mapping to a one-body Lagrangian mechanics, where DPTs are identified as non-analytic points in a minimization of an action. Moreover, an experimental setup is proposed to observe an analog of DPTs in linear, rather than exponential time.

This paper is organized as follows. In Sec. II we briefly recapitulate the MFT and the AP conjecture, as well as the analogy to Lagrangian mechanics. In Sec. III a few relevant models are considered to demonstrate the required essentials for a DPT. In Sec. IV we generalize the geometrical method to boundary-driven processes with a weak field. In Sec. V we summarize the results and discuss future directions. Moreover, an experimental setup is proposed in which the analog of DPTs can be directly observed.

II. THEORETICAL BACKGROUND

This section is devoted to summarizing the main points of the MFT leading to the AP conjecture. We will then present the mapping to Lagrangian mechanics, which will later prove useful to identifying DPTs.

Consider a lattice gas in a $1d$ system of L sites with diffusive dynamics. In the fluctuating hydrodynamic approach [48–50], we replace the microscopic space and time coordinates $i \in 1, \dots, L$ and t with hydrodynamic coordinates $x = i/L \in [0, 1]$ and $t' = t/L^2$. The relevant macroscopic variables are the particle and current densities $\rho(x, t')$, $j(x, t')$

*ohad.shpielberg@lpt.ens.fr

[7], related through the continuity equation

$$\partial_\tau \rho(x, t') = -\partial_x j(x, t'). \quad (2)$$

Connecting our system to two reservoirs at the boundaries $x = 0, 1$ with fixed densities ρ_l, ρ_r correspondingly, drives it out of equilibrium. The steady-state current J_S and steady-state density profile ρ_S of such a diffusive system obey Fick's law,

$$J_S = -D(\rho_S)\partial_x \rho_S. \quad (3)$$

Using Eq. (3) in Eq. (2) identifies D as the diffusion parameter of the (steady-state) diffusion equation. Assuming that the current density $j(x, t')$ can be described by small fluctuations around the steady state provides a description of the dynamics. This amounts to writing

$$j(x, t') = -D[\rho(x, t')]\partial_x \rho(x, t') + \sqrt{\frac{\sigma(\rho(x, t'))}{L}} \xi(x, t'), \quad (4)$$

with ξ a white noise in (x, t') , and $\sigma(\rho)$, the conductivity [7], characterizes the fluctuations.

Using the Martin-Siggia-Rose procedure [51] for Eq. (4), one finds that the probability to observe $\{\rho, j\}$ in time and space is given by

$$\mathcal{P}_i(\{\rho, j\}) \sim \exp\left(-L \int_0^1 dx \int_0^{t/L^2} dt' \mathcal{L}\right), \quad (5)$$

where $\mathcal{L} = \frac{1}{2\sigma(\rho)}[j + D(\rho)\partial_x \rho]^2$ and Eq. (2) is implicitly assumed. For large systems $L \gg 1$, observables obtained from \mathcal{P}_i are governed by a saddle point approximation. This implies that obtaining the LDF amounts to solving a minimization problem with two constraints; the continuity equation and particle transfer equals Q . Namely, $t \Phi(J) = L \min_{\rho, j} \int dx dt' \mathcal{L}$, with the constraints Eq. (2) and $Q = L^2 \int dx dt' j(x, t')$. Moreover, we consider only density profiles with fixed boundary conditions at $x = 0, 1$ corresponding to the reservoir densities. This formal minimization problem is hardly solvable in the general case as it involves solving a non-linear partial differential equation [44]. In Ref. [41], the AP conjecture was presented. It assumes that the solution to this optimization problem is time-independent, namely $j(x, t') = J$ and $\rho(x, t') \rightarrow \rho(x)$. As mentioned in Sec. I, this conjecture is particularly successful for boundary-driven processes. The AP solution satisfies both constraints and the LDF is now given by

$$\Phi(J) = \frac{1}{L} \min_{\rho} \int_0^1 dx \mathcal{L}_J(\rho, \partial_x \rho), \quad (6)$$

with $\mathcal{L}_J(\rho, \partial_x \rho) = (J + D\partial_x \rho)^2/2\sigma$. From Eq. (6), the LDF is recovered as a solution of an ordinary differential equation. A significant improvement to solving a partial differential equation. Throughout the text, we assume the AP solution is valid (see Ref. [45] for a counter-example).

To present the Lagrangian mechanics analogy, let us redefine $s = xJ$, $\tau = J$, and $W = L\Phi(J)/J$. Then, Eq. (6) becomes

$$W(\tau) = \min_{\rho} \int_0^{\tau} ds \mathcal{L}_1(\rho, \partial_s \rho), \quad (7)$$

with $\mathcal{L}_1 = (1 + D\partial_s \rho)^2/2\sigma$. W can be interpreted as the minimal action of a particle to travel between the position ρ_l at time $s = 0$ to the position ρ_r in time $s = \tau$. Finding $W(\tau)$ requires solving the Euler-Lagrange equation for the trajectory $\rho(s)$ constrained at the initial and final time. These Dirichlet boundary conditions allow for multiple solutions. Assume that for $i = 1, 2$ there are two solutions of the Euler-Lagrange equation denoted by $\rho_i(s)$ with $W_i \equiv \int ds \mathcal{L}_1(\rho_i, \partial_s \rho_i)$. If there exists τ_C such that $W_1 < W_2$ for $\tau < \tau_C$ and $W_1 > W_2$ for $\tau > \tau_C$, $W = \min\{W_1, W_2\}$ is a nonanalytic function at τ_C . We identify such nonanalytic points as DPTs [52].

A general solution of the Euler-Lagrange equation is hard to obtain. Moreover, our goal is to identify DPTs using nonperturbative geometrical considerations, without solving differential equations. To do so, we consider the Hamiltonian H corresponding to \mathcal{L}_1 . With the canonical variables ρ, Π (see Appendix A), we find $H(\rho, \Pi) = E_k + V(\rho)$. Interpreting $E_k = \frac{1}{2m}\Pi^2$ as the ‘‘kinetic energy’’ with the nonnegative mass $m = \frac{D^2}{\sigma}$, and the ‘‘potential’’ $V = -1/2\sigma$. The particle's trajectory is determined by the Hamilton equations. Let us relax the Dirichlet boundary conditions and instead use Cauchy boundary conditions to uniquely determine the trajectory $\rho(s)$. Namely, set $\rho(s = 0) = \rho_l, \Pi(s = 0)$ and find the corresponding τ values (if any exist) for which $\rho(s = \tau) = \rho_r$. Varying $\Pi(s = 0)$ allows to obtain all possible solutions. Then, we may evaluate W as (see Appendix A)

$$W(\tau) = \int_0^{\tau} ds [E_k - V + \Pi(-2V/m)^{1/2}]. \quad (8)$$

The Hamilton equations are by no means easier than the Euler-Lagrange equations. However, all the solutions can be identified from the geometry of the potential using the Cauchy boundary conditions.

III. DYNAMICAL PHASE TRANSITIONS

In what follows, we analyze the possible solutions of Eq. (7) and decide whether DPTs can occur in a toy model, defined at the macroscopic level only. This model highlights the advantages of the Hamiltonian approach. Physically relevant models will be discussed in Sec. IV, Sec. V, and Appendix E. The analysis goes as follows. Identify the possible solutions for some boundary conditions. If more than one solution exists, evaluate $W(\tau)$ for the solutions at $\tau \rightarrow 0, \infty$. If different solutions become optimal at the different limits $\tau \rightarrow 0, \infty$, there is a DPT.

It will become clear that cyclic trajectories, i.e., $\hat{\rho} = \rho_l = \rho_r$, provide ample intuition where to search for DPTs. Therefore, we focus on cyclic trajectories in the main text. Two acyclic trajectories are analyzed in a similar manner in Appendix D. We analyze only the cases where $\tau > 0$. A similar, time-reversed analysis can be made. However, due to the Gallavotti-Cohen relation [53], the optimal density profiles are identical to the time-reversed solutions (for any boundary conditions). The negative current part of LDF can be inferred from the positive current part [16,41]. Moreover, we note that no new behavior can be obtained by switching $\rho_l \leftrightarrow \rho_r$, as this is merely conditioning the time-reversed process. In what follows, the sign of Π corresponds to the direction of the ρ

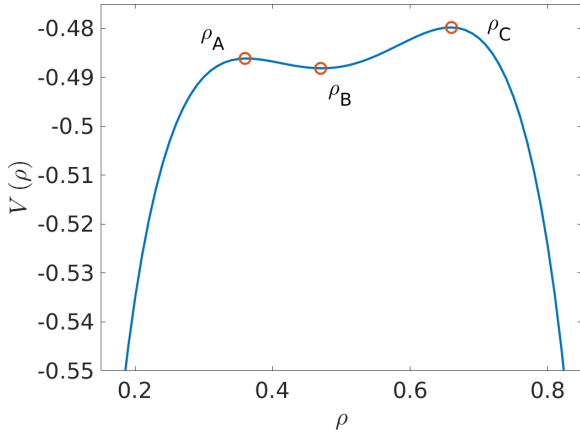


FIG. 1. The potential for AMFH model with $B = -20, \epsilon = 0.02$ (solid blue line). The extremal points are marked in (red) circles, where $\rho_A(\rho_C)$ is the lower (higher) peak and ρ_B is the local minimum.

axis (see Fig. 1). Moreover, we identify different solutions by setting $\Pi_0 = \Pi(s = 0)$ at the initial time, which, together with the initial position ρ_l determines the energy H . In this section, only analytical mechanics arguments will be invoked.

The asymmetric Mexican flat hat (AMFH) model [45] is a toy model, used here to demonstrate how to identify DPTs under the AP assumption. We define macroscopically using $D = 1$ and

$$\sigma = \left(\rho - \frac{1}{2}\right)^2 + B\left(\rho - \frac{1}{2}\right)^4 - \frac{B+4}{16} + \epsilon\rho^2(1-\rho). \quad (9)$$

For $B = -20$ and $\epsilon = 0.02$, the potential of the AMFH model presents three extremal points at ρ_A, ρ_B, ρ_C (see Fig. 1). We analyze three of the seven cyclic boundary conditions cases. The four remaining cases are left to Appendix B. A few acyclic processes are analyzed in Appendix D in a similar manner.

Case 1, $\hat{\rho} = \rho_A$: Here, there are at least two distinct trajectories. In the first, the particle stays put. Namely, $\rho(s) = \rho_A$ and $\Pi(s) = 0$. This solution is viable for any τ . From Eq. (8) we find that the action associated with this trajectory is $W_{\text{put}}(\tau) = -\tau V(\rho_A)$. In the second possible trajectory, $\Pi_0 > 0$. This implies $\tau(H) \in [\tau_0, \infty)$ for the energy $H \in (V(\rho_A), V(\rho_C))$. Here $\tau_0 > 0$ is the minimal time it takes the particle to cross the second trajectory, going from ρ_A to climb the potential hump of ρ_C (never crossing it) and then travel back. We can further evaluate from Eq. (8) the action corresponding to the second trajectory for $H \rightarrow V(\rho_C)$, $\Pi_0 > 0$, which corresponds to $\tau \rightarrow \infty$. We find that this action is $W_2(\tau) = -\tau V(\rho_C) + O(1)$ as the particle spends most of the time approaching ρ_C . While for short times W_{put} is the sole and hence the dominant trajectory, we found that for some large but finite τ , the second trajectory dominates. Therefore, W is nonanalytic and a DPT takes place. We note that such a DPT could not be obtained using a perturbative approach [44,47].

Case 2, $\hat{\rho} < \rho_A$: Here there are again at least two possible trajectories, both with $\Pi_0 > 0$. We denote the first trajectory as the short path. It corresponds to $\tau_{\text{short}}(H) \in [0, \infty)$ for $H \in [V(\hat{\rho}), V(\rho_A))$, where the particle never crosses the lower

potential peak at ρ_A . In the long path, the particle crosses the potential peak at ρ_A , but not the one at ρ_C . This corresponds to $\tau_{\text{long}}(H) \in [\tau_0, \infty)$ for $H \in (V(\rho_A), V(\rho_C))$. τ_0 is the minimal finite time it takes the particle to complete the long trajectory (not the same value as in case 1). At long times, we can evaluate the action of the short path using Eq. (8). We find $W_{\text{short}} = -\tau V(\rho_A) + O(1)$. Similarly, we can evaluate the action of the long path for $H \rightarrow V(\rho_C)$. We find $W_{\text{long}} = -\tau V(\rho_C) + O(1)$. So, while W_{short} dominates at short times $\tau < \tau_0$, W_{long} dominates at long times and a DPT must occur.

Case 3, $\hat{\rho} = \rho_B$: Here, there are infinitely many distinct trajectories. Let us characterize them. The first possibility is staying put as the particle sits on a potential extremum. The solution is valid for any time τ with an associated action $W_{\text{put}}(\tau) = -\tau V(\rho_B)$. We note that this is the only trajectory allowing for $\tau \rightarrow 0$. A second possible solution is for the particle to pick up some initial positive (negative) momentum Π_0 . Even for infinitely small momentum, the minimal time τ_0 to cross the path (going slightly up the potential and back down to ρ_B) is finite. The motion is essentially that of half a cycle of an harmonic oscillator. Solving the harmonic oscillator equations of motion around the point ρ_B , we find that $\tau_0 = \pi \sqrt{\frac{m(\rho_B)}{\partial_{\rho\rho} V(\rho_B)}}$. If a transition between the “staying put” trajectory to this one occurs, it can be a continuous transition. A transition indeed occurs in this case exactly at τ_0 . it can be validated by numerically solving the Hamilton equations (Appendix G), or analytically using a perturbative approach [47]. We note that one can evaluate the order of magnitude of τ_0 by using a harmonic oscillator approximation for any of the cases studies for the AMFH model. We can also consider multiple crossings of ρ_B as long as the energy does not exceed $V(\rho_A)$. Considering $\Pi_0 > 0$ with $H \rightarrow V(\rho_C)$ amounts to $W_{\text{right}}(\tau) = -\tau V(\rho_C) + O(1)$ for $\tau \rightarrow 0$. This trajectory is certainly preferable to the “staying put” trajectory and thus we may have a richer phase diagram. While the geometrical approach does not help to obtain the full phase diagram, it certainly verifies that a DPT indeed occurs in this scenario.

A numerical verification for the DPTs found here and in Appendix B was performed in a similar manner to that explained in the Appendix of Ref. [45]. We also note that as in other cases, multiple transitions may occur. Case 2 dispels any illusion that DPTs are related to boundary conditions on or close to extremal points of σ .

To conclude, we found that extremal points in the potential (conductivity) are facilitators of DPTs. It should be clear that similar arguments can be invoked to identify DPTs for acyclic trajectories. In the corresponding MFT picture, the particle trajectories are density profiles. Figure 2 depicts the density profiles for small and large positive values of the current J (short and long time τ) for the first two cases discussed in this section.

IV. GENERALIZATION TO MODELS WITH WEAK FIELDS

Let us now consider the macroscopic fluctuation theory for models with a weak asymmetry in the form of a field of strength E . The Einstein relation implies that Fick’s law Eq. (3) is modified to include the asymmetry by the addition of a $E\sigma$

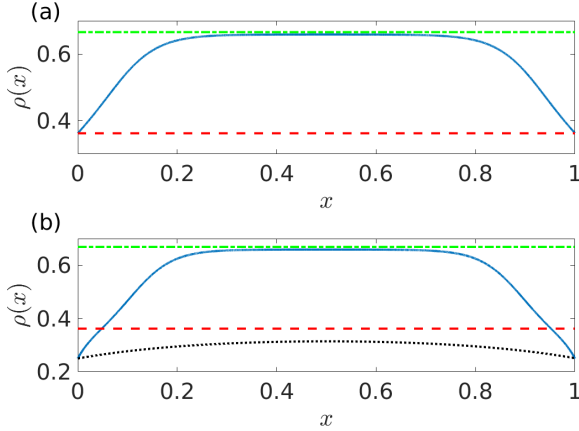


FIG. 2. Typical density profiles in the AMFH model. (a) Case 1, $\hat{\rho} = \rho_A$, the (red) dashed line corresponds to the staying put trajectory and the (blue) solid line corresponds to the second trajectory at large currents (large τ). It begins to saturate ρ_C represented by the (green) dashed-dotted line as expected. (b) Case 2, $\hat{\rho} < \rho_A$, the (blue) dotted line corresponds to the short trajectory for low values of the current ($\tau < \tau_0$) and the (red) solid line corresponds to the long trajectory at large currents ($\tau > \tau_0$). It begins to saturate ρ_C represented by the (green) dashed-dotted as expected.

term. Repeating the same procedure of the fluctuating hydrodynamics and assuming the AP, we find that the Lagrangian in Eq. (6) is modified to $\mathcal{L}_J = (J + D\partial_s\rho + E\sigma)^2/2\sigma$. Then, going to the Lagrangian mechanics, we find that Eq. (7) is given with $\mathcal{L}_1 = (1 + D\partial_s\rho + \tilde{E}\sigma)^2/2\sigma$ with the rescaled field $\tilde{E} = E/\tau$. Thus, in principle, the potential changes as a function of our end-time τ . This in turn allows to identify more DPTs, albeit in a more subtle way. Moreover, notice that for $\tau \rightarrow \infty$, the action loses its dependency of the field E . The Hamiltonian here is given by the same form with the same mass term. The generalized momentum $\Pi = \frac{\partial \mathcal{L}_1}{\partial \dot{\rho}} - \frac{D}{\sigma} - D\tilde{E}$ and the potential is $V(\rho) = -\frac{1}{2\sigma}(1 + \tilde{E}\sigma)^2$. The action W in Eq. (8) remains of the same form. Our course of action will be only slightly different than the zero field case. First, we will identify initial and final conditions where for $\tau \rightarrow \infty$ and $\tilde{E} \rightarrow 0$ there is a single solution. Then, for finite τ and large \tilde{E} , we identify another solution in addition to the large τ solution. This new solution will be argued to dominate, namely it has a smaller action. As before, this guarantees a DPT. It should be noted that while there is freedom in the selection of E , once chosen, it is kept fixed throughout the process, at least in our specific setup.

The weakly asymmetric simple exclusion process

The simple symmetric exclusion process (SSEP) is a paradigm process for nonequilibrium systems as it is solvable by Bethe ansatz [7,54]. In the SSEP, there is at most one particle per site, and particles hop to empty neighbors with rate 1. This implies $D = 1$ and $\sigma = 2\rho(1 - \rho)$. The large deviation function is known to be analytic, so no DPTs occur. In the weakly asymmetric simple exclusion process (WASEP), particles hop to empty sites to the right (left) with rate $1 \pm E/L$. The scaling of the field with the system size keeps the process diffusive. To identify DPT, we draw the

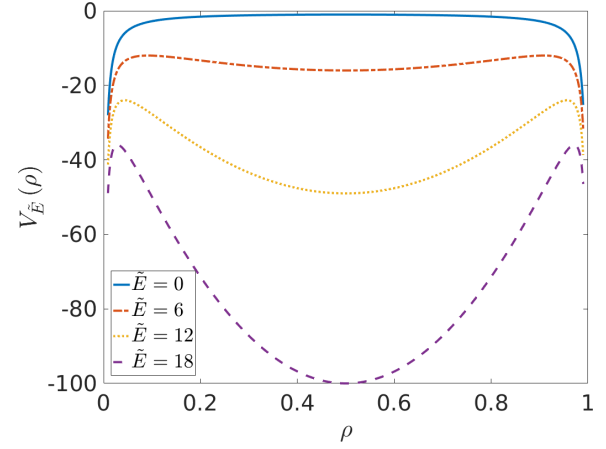


FIG. 3. The corresponding potentials for various values of \tilde{E} of the WASEP. It can be seen that the basic structure of the potential is completely changed for different values of \tilde{E} . For $|\tilde{E}| > 2$, there are two maxima at $\rho_{\pm} = \frac{1 \pm \sqrt{1 - 2/|\tilde{E}|}}{2}$ and one minimum at $\rho = 1/2$, whereas for $|\tilde{E}| < 2$ there is a single maximum at $\rho = 1/2$. This behavior give rise to the DPTs discussed in the main text.

potential of the WASEP for several values of \tilde{E} (see Fig. 3). We specify two cases of interest.

Case 1, $\hat{\rho} = 1/2$: In the SSEP, there is an obvious particle hole symmetry and therefore this is an immediate point of interest. For $\tilde{E} \rightarrow 0$ which corresponds to the limit $\tau \rightarrow \infty$, there is a single trajectory. Namely, staying put $\rho(s) = 1/2$ with $\Pi(s) = 0$ (see Fig. 3). For $\tilde{E} \gg 1$ there are more solutions. Staying put remains a solution. Another solution is for the particle to start climbing the potential and then tumble back. We have already seen in Sec. III case 3, that if τ is large enough this solution is dominant. Since we still have the freedom to choose E , we can always have \tilde{E} large while keeping a large enough τ . Thus, we expect a DPT at large values of E . This case was also discussed in Ref. [47].

Case 2, $0 < \rho_l < 1/2$ and $\rho_r = 1 - \rho_l > 1/2$: For $\tilde{E} \rightarrow 0$ which corresponds to the limit $\tau \rightarrow \infty$, there is again a single trajectory. The particle must have $\Pi_0 > 0$ large enough to overcome the potential barrier. However, for $|\tilde{E}| > 2$, the potential is completely changed as two new maxima appear (at $\rho_{\pm} = \frac{1 \pm \sqrt{1 - 2/|\tilde{E}|}}{2}$) and the old maximum becomes a minimum. Now, suppose that \tilde{E} is such that ρ_l, ρ_r are located between the two maxima. Then, we may focus on two trajectories. The direct one with $\Pi_0 > 0$ and the indirect where the particle has $\Pi_0 < 0$ and it starts climbing towards the left maximum of the potential. For the direct path, $W_{\text{direct}} \geq -\tau V(\rho_l)$, as $E_k, \Pi > 0$ in this trajectory. For the indirect path at the long time limit, we can evaluate $W_{\text{indirect}} = -\tau V(\rho_{\pm}) + O(1)$. Since we have picked ρ_l such that $V(\rho_{\pm}) > V(\rho_l)$ a DPT must occur as $W_{\text{indirect}} < W_{\text{direct}}$. So, like in case 1 above, we can always choose E that allows τ to be large enough for the desired value of \tilde{E} . This guarantees a DPT. In fact, we need not require any symmetry between ρ_l and ρ_r to observe the transition as we choose \tilde{E} such that $V(\rho_{\pm}) > V(\rho_{l,r})$. Therefore, a transition should be expected for any choice of $\rho_l < \frac{1}{2} < \rho_r$ for a sufficiently large E .

The large deviation function of the SSEP is known to be analytic [41,48,55]. We have seen that applying a weak field may generate new extremal points in the effective potential, thus allowing for DPTs. However, adding a weak field to a model will not necessarily generate DPTs for any model. One such counter example is for non-interacting Random walkers, where a single solution was obtained for any weak field [27]. While the potential may possess a local maximum point, it is not enough to identify a DPT using the geometrical approach.

V. DISCUSSION

We have presented here a mapping between current fluctuations in boundary-driven systems under the AP assumption to the evolution of a Hamiltonian particle with set initial and final positions. We have then shown that a pictorial analysis of the potential is sufficient to demonstrate DPTs. Note that the Hamiltonian approach allows to focus on the geometry of the potential, rather than exact details. While the AMFH model is a toy model, the conclusions presented above apply for models with similar conductivity, e.g., Bodineau's long-range hopping model [44,45] and the Katz-Lebowitz-Spohn model [47,56–58]. See Appendix E for details on these two processes. This approach allows to obtain new DPTs, as well as derive on simple terms known DPTs [45,47].

The geometrical approach provides a sufficient condition for DPTs. We found that extremal points in the potential are facilitators of DPTs. One can wrongly assert that, since the diffusion does not play a role in the potential, it is immaterial to the study of DPTs. However, aside from affecting the value of the critical current (or corresponding time τ), the diffusion may allow for a richer phase diagram (see cases D and E in Appendix B and Ref. [47] for examples). It cannot be ruled out that the nontrivial mass term facilitates a DPT that cannot be identified from the potential. Such DPTs are outside the scope of this paper and are not neatly described by the formalism presented here.

We further note that once a DPT is identified using the Lagrangian approach, the order of magnitude of the transition ($\sim\tau_0$) can be recovered from dimensional analysis of the mass and potential (Sec. III, Case 3).

The method was extended to include weak driving fields. We have shown that the potential explicitly depends on the ratio of the applied field and the current. This allows for more extremal points to be generated for different values of the field and thus it enables more DPTs.

In Appendix F, we have generalized the geometrical approach to the case of d different species of particles. This corresponds to Lagrangian mechanics of a single particle in d spatial dimensions. Similarly to the case of a boundary-driven process with a weak field, more control parameters are included (more than one constrained current). This implies that in principle, DPTs should be found in abundance for physical models with interacting particle species as the control parameters can be used to generate more extremal points in the potential.

Finally, an experimental setup realizing the analog of the LDF can be considered. Direct experimental measurement of the LDF is hard as we are searching for exponentially rare events. Finding a mechanical system described by the

effective Hamiltonian H allows to experimentally probe $W(\tau)$, the equivalent of the LDF. As the mapping suggests atypical currents $J \rightarrow \tau$, we find that an analog Hamiltonian explores large deviations in linear time. This exponential reduction is due to the AP, allowing to discard many trajectories (see Ref. [59] for similar motivation).

One possible realization is by lacing a bead of mass m , susceptible to gravity g , through a hard string. Negligible dissipation of energy is assumed throughout the process. The string's contour is given by $\vec{r} = [x, f(x), h(x)]$. Thus, the corresponding Hamiltonian is $H = \frac{1}{2m}(\Pi_x^2 + \Pi_z^2 + \Pi_y^2) - mgz$. Hamilton equations dictate $\Pi_y = \Pi_x \partial_x f(x)$ and $\Pi_z = \Pi_x \partial_x h(x)$. This amounts to rewriting an effective 1d Hamiltonian $H_{\text{eff}} = \frac{1}{2m_{\text{eff}}}\Pi_x^2 - mgh(x)$, with $m/m_{\text{eff}} = 1 + (\partial_x f)^2 + (\partial_x h)^2$. Control over f, h allows to replicate the desired space-dependent effective mass and potential in a finite range for a variety of D, σ functions (see Appendix C).

Note that there is no clear advantage to finding W experimentally rather than a numerical evaluation. However, this example shows that DPTs could be observed experimentally in linear time using analog systems. This idea motivates searching for the equivalent of the AP in other large deviation problems.

ACKNOWLEDGMENTS

This work has been supported by ANR Grant No. 14-CE25-0003. O.S. thanks Y. Don, D. Bernard, T. Nemoto, B. Timchenko, and J. Troost for useful discussions, comments, and ideas.

APPENDIX A: HAMILTONIAN FORMALISM

In this section we derive, for completeness, the Hamiltonian H corresponding to the Lagrangian \mathcal{L}_1 of the main text. We define, as usual, H as the Legendre transform of \mathcal{L}_1 . Namely, $H = p\partial_s q - \mathcal{L}_1$, with $p = \frac{\partial \mathcal{L}_1}{\partial(\partial_s \rho)}$. We find

$$H = \frac{1}{2m}\Pi^2 + V, \quad (\text{A1})$$

where $\Pi = p - D/\sigma$, $m = D^2/\sigma$, and $V = -1/2\sigma$. Notice ρ, Π are canonical. Defining $E_k = \frac{1}{2m}\Pi^2$ as the kinetic term allows us to identify (as usual) the total energy as the sum of the kinetic and potential energies. Note that $\Pi = m\partial_s \rho$, which implies that zero kinetic energy makes for vanishing "velocity" $\partial_s \rho$. We can thus rewrite the Lagrangian (in an unusual way)

$$\mathcal{L}_1 = E_k - V + \Pi\sqrt{-2V/m}. \quad (\text{A2})$$

APPENDIX B: ANALYSIS OF EQUAL BOUNDARY CONDITIONS FOR THE AMFH MODEL

This section deals with the case of equal boundary condition for the AMFH model, i.e., $\hat{\rho} = \rho_l = \rho_r$. In the main text, three out of possible seven cases were discussed. Here, we complete the discussion by analyzing the remaining four cases. ρ_A, ρ_B, ρ_C are depicted in Fig. 1 of the main text.

Case 4, $\rho_A < \hat{\rho} < \rho_B$: Similarly to Case 3, we find in Case 4 infinitely many solutions as the particle may revisit $\hat{\rho}$ several times. Let us focus on two solutions: the short-left and

short-right. In the short-left solution, $\Pi_0 \leq 0$. $\tau_{\text{left}}(H) \in [0, \infty)$ for $H \in [V(\hat{\rho}), V(\rho_A))$. In the short-right solution, $\Pi_0 > 0$ and $\tau_{\text{right}}(H) \in (\tau_0, \infty)$ for $H \in (V(\hat{\rho}), V(\rho_C))$. $\tau_0 > 0$ is the minimal finite time for the particle to traverse the short-right trajectory. For $\tau \rightarrow \infty$, the particle traveling in the short-left (right) trajectory spends most of its time approaching the peak at $\rho_A(\rho_C)$ with vanishing kinetic energy. In the similar manner to the main text, evaluating Eq. (8) implies $W_{\text{left}} > W_{\text{right}}$ as $\tau \rightarrow \infty$.

One can also consider trajectories that cross $\hat{\rho}$ more than once as the particle can perform an oscillatory motion. They compose an infinite set of solutions. To find the complete phase diagram, one has to pursue a detailed analysis. However, only the short-left trajectory is viable for $\tau \rightarrow 0$. Since the short-right solution dominates over the short-left solution at long times, a DPT is guaranteed.

Note that here, the phase diagram may be richer due to the infinite set of solutions at intermediate times. A detailed analysis to recover the full phase diagram is not attempted here.

Case 5, $\rho_B < \hat{\rho} < \rho_C$: This case is very similar to Case C. Here, however, there is no guarantee for a DPT, as for short and long times the short-right path is favorable ($\Pi_0 > 0$). The intermediate times must be analyzed with care and cannot be inferred from this simple picture.

Case 6, $\hat{\rho} = \rho_C$: Here there is only one possible solution, staying put. The particle never returns to ρ_C for any nonzero Π_0 . So, no DPT is expected.

Case 7, $\hat{\rho} > \rho_C$: Here again there is only a single possible solution with $\Pi_0 < 0$. Therefore, no DPT can be identified from the potential alone.

APPENDIX C: EXPERIMENTAL MODELING

We have shown in the main text that hard string laced through a bead can give a prescription for a desired 1d effective dynamics. The purpose is to find for arbitrary D, σ , the contour of the string giving rise to the effective Hamiltonian. First, notice that the important parameters in the experiment are the mass of the bead m the gravity constant g and a characteristic length scale x_0 . Therefore, we attribute dimensions to $D(x)$ and $\sigma(x)$ for the model to make physical sense,

$$\sigma(x) = \frac{1}{mgx_0}\sigma(\rho),$$

$$D(x) = \frac{1}{\sqrt{gx_0}}D(\rho),$$

with $\rho = x/x_0$, $D(\rho)$, and $\sigma(\rho)$ dimensionless parameter and functions. We can thus write $h(x) = x_0h(\rho)$ and $f(x) = x_0f(\rho)$. Since $V = mgh(x) = 1/2\sigma(x)$, we find $h(\rho) = 1/2\sigma(\rho)$. We use the effective mass equation to find $\partial_\rho f(\rho)$ by

$$[\partial_\rho f(\rho)]^2 = \frac{\sigma(\rho)}{D^2(\rho)} - 1 - \frac{1}{4} \frac{[\partial_\rho \sigma(\rho)]^2}{[\sigma(\rho)]^4}. \quad (\text{C1})$$

Unfortunately, the right-hand side of Eq. (C1) is not always positive. For example, for the AMFH model, we find that the right hand side of Eq. (C1) is in fact always negative. However, recall that the DPTs are dominated by the potential, and the

role of the diffusion $D(\rho)$ is secondary. So, changing D to, e.g., $D = [(1 - \rho)\rho]^4$ allows us to find a real function $f(\rho)$ in for any $\rho \in [0, 1]$. We note that the potential can never be truly mimicked as $V(\rho \rightarrow 0) \rightarrow -\infty$ is experimentally unreachable. This toy model provides merely a proof of principle. One can compose a variety of potentials using, e.g., electric fields to try and mimic the desired Hamiltonian for arbitrary D, σ . This will not be attempted here.

APPENDIX D: ACYCLIC TRAJECTORIES FOR THE AMFH MODEL

To complete the discussion in Sec. III we discuss possible DPTs for two cases of acyclic paths in the AMFH model. Namely, the reservoirs are taken at different densities.

Case 1, $\rho_l < \rho_A$ and $\rho_A < \rho_r < \rho_B$: Here, there is always a direct trajectory where $\Pi_0 > 0$ with $H \in (V(\rho_A), \infty)$. The particle passes over the ρ_A potential peak and directly continues to ρ_r . Here, larger energies H correspond to smaller time values τ . Any τ value is viable. A second possible solution is again for $\Pi_0 > 0$, with $H \in (V(\rho_A), V(\rho_C))$. Here the particle crosses ρ_l once as it starts to climb towards ρ_C , only to tumble back down towards ρ_l . Here there is some minimal finite time τ_0 , below which the trajectory cannot be realized. This ensures that the direct trajectory dominates at short times. Evaluating Eq. (8) ensures that the direct trajectory is no longer dominant at large enough times. Therefore, we have identified a DPT.

Case 2, $\rho_l = \rho_A$ and $\rho_r = \rho_C$: Here it is easy to understand that there is only a single trajectory possible to reach from ρ_A to ρ_C . This means we cannot identify a DPT from the geometrical approach. Of course, this does not exclude a DPT altogether.

APPENDIX E: PHYSICAL MODELS THAT SUPPORT DPTs

Let us present here in more detail two physically relevant models that reproduce the discussed DPTs of the main text.

1. The long-range hopping with exclusion model

This model, proposed by Bodineau [44,45], is a one-dimensional lattice-gas model with at most one particle per lattice site. A particle can hop from site i to an empty nearest-neighbor site $i \pm 1$ with rate 1 and it is also allowed to hop from site i to an empty site $i \pm (\beta + 1)$ with rate α provided that the β sites separating them are all occupied. D and σ can be obtained analytically as this is a gradient model [60]. We obtain $D(\rho) = 1 + \alpha(\beta + 1)^2\rho^\beta$ and $\sigma(\rho) = 2\rho(1 - \rho)D(\rho)$ with $\rho \in [0, 1]$. Choosing $\alpha = \frac{1}{24}$ and $\beta = 9$ allows us to reproduce the double peaked potential as shown in Fig. 4. This of course allows us to reproduce the DPTs discussed in the main text.

2. The Katz-Leibowitz-Spohn model

The Katz-Leibowitz-Spohn [56,57] model is a lattice gas model with exclusion, that incorporates nearest-neighbor hopping with interactions. The dynamics of right-handed hopping is given below, where full circles represent occupied

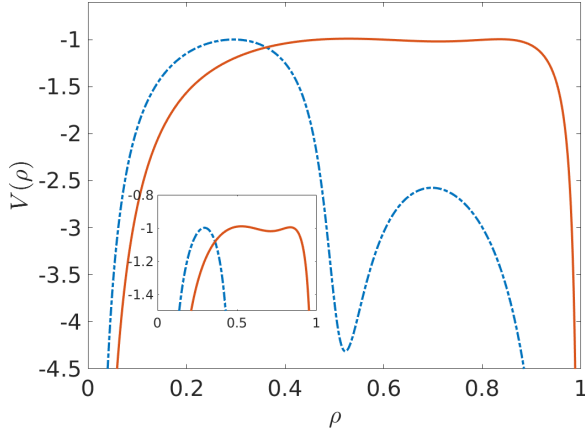


FIG. 4. The corresponding potentials for the Long-range hopping model with $\alpha = \frac{1}{24}, \beta = 9$ (solid red line) and the KLS model with $\delta = 0.45, \epsilon = 0.99$ (dashed blue line). The inset shows a zoom-in on the extremal points structure of the Long-range hopping model.

sites and empty circles represent empty sites:



The spatially inverted transitions occur with identical rates. The parameters ϵ, δ provide some control over D, σ , where exact expressions are given in the Appendix of Ref. [47]. By choosing, e.g., $\epsilon = 0.99, \delta = 0.45$, we can obtain the desired double peaked potential to reconstruct the DPTs discussed in the main text (see Fig. 4)

APPENDIX F: MULTI-SPECIES MODELS

In this section we show how to extend the Hamiltonian approach to one-dimensional boundary-driven systems with d different species of particles. Here again, we consider all the different species are conserved in the bulk, namely, $\partial_t \rho_\alpha = -\partial_x j_\alpha$ for $\alpha = 1 \dots d$. We also consider a generalized stochastic Fick's law of the form $j_\alpha = q_\alpha + \sqrt{\frac{\sigma_{\alpha\beta}}{L}} \xi_\beta$, where the conductivity σ determines the strength of the fluctuations and q_α determines the mean current. To make matters simple, we consider q_α of the form

$$q_\alpha = -D_{\alpha\beta} \partial_x \rho_\beta, \quad (\text{F1})$$

where $D_{\alpha\beta}$ is the diffusion matrix. We can thus obtain a Lagrangian of the form

$$\mathcal{L} = \frac{1}{2} \sigma_{\alpha\beta}^{-1} (j_\alpha + q_\alpha)(j_\beta + q_\beta), \quad (\text{F2})$$

where σ^{-1} is the inverse of the conductivity matrix.

Now, using the AP, we take $j_\alpha(x, t) \rightarrow J_\alpha$ and $\rho_\alpha(x, t) \rightarrow \rho_\alpha(x)$. As usual, we rescale $x \rightarrow s = x J_1 \in [0, \tau]$, such that we want to find

$$W(\tau) = \int_0^\tau ds \mathcal{L}_{1d}, \quad (\text{F3})$$

where $\mathcal{L}_{1d} = \frac{1}{2} \sigma_{\alpha\beta} (r_\beta + q_\beta)(r_\beta + q_\beta)$, with $r_\alpha = J_\alpha / J_1$. The corresponding Hamiltonian to \mathcal{L}_{1d} is

$$H_{1d} = E_K + V, \quad (\text{F4})$$

with

$$\begin{aligned} E_K &= \frac{1}{2} m_{\alpha\beta}^{-1} \Pi_\alpha \Pi_\beta, \\ V &= -\frac{1}{2} r_\alpha r_\beta \sigma_{\alpha\beta}^{-1}, \end{aligned} \quad (\text{F5})$$

where we have defined

$$m_{\mu\nu} = D_{\alpha\mu} \sigma_{\alpha\beta}^{-1} D_{\beta\nu}. \quad (\text{F6})$$

As usual, Π_α are canonical variables to ρ_α and $W(\tau)$ is also given by

$$\mathcal{L}_{1d} = E_k - V + \sigma_{\alpha\beta}^{-1} D_{\alpha\gamma} m_{\eta\gamma}^{-1} r_\beta \Pi_\eta. \quad (\text{F7})$$

One can verify that Eq. (F7) becomes Eq. (8) for a single species of particles. Identifying a DPT can be done in a similar fashion to what was done in Secs. III and IV. However, finding and analyzing a microscopic model that presents such a transition is beyond the scope of this paper.

APPENDIX G: NUMERICAL VERIFICATIONS

In this section we present numerical verifications for cases 1 and 3 of the AMFH model in Sec. III. We numerically solve the Hamilton equations with the Cauchy boundary conditions. Namely, we set the initial conditions $\rho(s=0) = \rho_l$ and $\Pi(s=0) = \Pi_0$. We vary Π_0 to set the energy H within the allowed range of the desired trajectory. We identify τ to satisfy $\rho(\tau) = \rho_r$. Note that for a trajectory of choice we already determine how many times $\rho(s)$ visits ρ_r as τ need not be the first time $\rho(s) = \rho_r$.

The plots of $W(\tau)$ for the different trajectories are shown in Fig. 5.

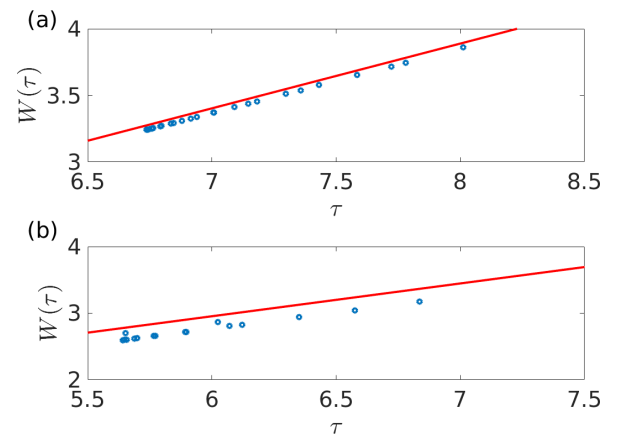


FIG. 5. The numerical values for the action $W(\tau)$ for two possible solutions are considered. (a) corresponds to Case 1 and (b) to Case 3 in Sec. III. The (red) curve represents the action $W(\tau)$ in the “staying put” solution and the (blue) circles correspond to the action $W(\tau)$ of the positive initial momentum Π_0 solution. In both cases, the positive initial momentum solution becomes dominant as soon as it is feasible [i.e., $\tau_0 = 6.7(5.6)$ for case 1 (3), correspondingly].

- [1] K. G. Wilson and J. Kogut, *Phys. Rep.* **12**, 75 (1974).
- [2] J. M. Yeomans, *Statistical Mechanics of Phase Transitions* (Clarendon Press, Oxford, 1992).
- [3] J. M. Kosterlitz and D. J. Thouless, *J. Phys. C: Solid State Phys.* **6**, 1181 (1973).
- [4] S. Sachdev, *Quantum Phase Transitions* (John Wiley, New York, 2007).
- [5] H. B. Callen, *Thermodynamics and an Introduction to Thermostatistics*, 2nd ed. (John Wiley, New York, 1985).
- [6] L. D. Landau, E. M. Lifshitz, and L. P. Pitaevskii, *Statistical Physics, Part I*, Course of Theoretical Physics, Vol. 5 (Pergamon Press, Oxford, 1980).
- [7] B. Derrida, *J. Stat. Mech.: Theory Exp.* (2007) P07023.
- [8] K. Mallick, *Physica A* **418**, 17 (2015).
- [9] A. Aminov, G. Bunin, and Y. Kafri, *J. Stat. Mech.: Theory Exp.* (2014) P08017.
- [10] L. Bertini, A. De Sole, D. Gabrielli, G. Jona-Lasinio, and C. Landim, *J. Stat. Mech.* (2010) L11001.
- [11] T. Bodineau and B. Derrida, *Phys. Rev. E* **72**, 066110 (2005).
- [12] C. Appert-Rolland, B. Derrida, V. Lecomte, and F. van Wijland, *Phys. Rev. E* **78**, 021122 (2008).
- [13] N. Tizón-Escamilla, P. I. Hurtado, and P. L. Garrido, *Phys. Rev. E* **95**, 032119 (2017).
- [14] N. Tizón-Escamilla, C. Pérez-Espigares, P. L. Garrido, and P. I. Hurtado, *Phys. Rev. Lett.* **119**, 090602 (2017).
- [15] L. Zarfaty and B. Meerson, *J. Stat. Mech.: Theory Exp.* (2016) 033304.
- [16] L. Bertini, A. De Sole, D. Gabrielli, G. Jona-Lasinio, and C. Landim, *Rev. Mod. Phys.* **87**, 593 (2015).
- [17] L. Bertini, A. De Sole, D. Gabrielli, G. Jona-Lasinio, and C. Landim, *Phys. Rev. Lett.* **87**, 040601 (2001).
- [18] L. Bertini, A. De Sole, D. Gabrielli, G. Jona-Lasinio, and C. Landim, *J. Stat. Phys.* **135**, 857 (2009).
- [19] L. Bertini, A. De Sole, D. Gabrielli, G. Jona-Lasinio, and C. Landim (2007), [arXiv:0705.2996](https://arxiv.org/abs/0705.2996).
- [20] A. Aminov, Y. Kafri, and M. Kardar, *Phys. Rev. Lett.* **114**, 230602 (2015).
- [21] L. Bertini, D. Gabrielli, G. Jona-Lasinio, and C. Landim, *Phys. Rev. Lett.* **110**, 020601 (2013).
- [22] P. Krapivsky, K. Mallick, and T. Sadhu, *J. Stat. Phys.* **160**, 885 (2015).
- [23] E. Akkermans, T. Bodineau, B. Derrida, and O. Shpielberg, *Europhys. Lett.* **103**, 20001 (2013).
- [24] T. Bodineau, B. Derrida, and J. L. Lebowitz, *J. Stat. Phys.* **140**, 648 (2010).
- [25] T. Bodineau, B. Derrida, and J. L. Lebowitz, *J. Stat. Phys.* **131**, 821 (2008).
- [26] T. Agranov, B. Meerson, and A. Vilenkin, *Phys. Rev. E* **93**, 012136 (2016).
- [27] O. Hirschberg, D. Mukamel, and G. M. Schütz, *J. Stat. Mech.: Theory Exp.* (2015) P11023.
- [28] T. Agranov and B. Meerson, *Phys. Rev. E* **95**, 062124 (2017).
- [29] P. I. Hurtado, A. Lasanta, and A. Prados, *Phys. Rev. E* **88**, 022110 (2013).
- [30] We could also consider continuous observables instead of discrete charge, e.g., heat.
- [31] D. Bernard and B. Doyon, *J. Phys. A: Math. Theor.* **45**, 362001 (2012).
- [32] B. Meerson, E. Katzav, and A. Vilenkin, *Phys. Rev. Lett.* **116**, 070601 (2016).
- [33] B. Derrida and Z. Shi, *J. Stat. Phys.* **163**, 1285 (2016).
- [34] T. Sadhu and B. Derrida, *J. Stat. Mech.: Theory Exp.* (2015) P09008.
- [35] H. Touchette, *Phys. Rep.* **478**, 1 (2009).
- [36] J. de Gier and F. H. L. Essler, *Phys. Rev. Lett.* **107**, 010602 (2011).
- [37] T. Bodineau and M. Lagouge, *J. Stat. Phys.* **139**, 201 (2010).
- [38] C. Giardinà, J. Kurchan, and L. Peliti, *Phys. Rev. Lett.* **96**, 120603 (2006).
- [39] P. I. Hurtado and P. L. Garrido, *Phys. Rev. Lett.* **102**, 250601 (2009).
- [40] T. Nemoto, E. G. Hidalgo, and V. Lecomte, *Phys. Rev. E* **95**, 012102 (2017).
- [41] T. Bodineau and B. Derrida, *Phys. Rev. Lett.* **92**, 180601 (2004).
- [42] L. Bertini, A. De Sole, D. Gabrielli, G. Jona-Lasinio, and C. Landim, *J. Stat. Phys.* **123**, 237 (2006).
- [43] P. I. Hurtado and P. L. Garrido, *J. Stat. Mech.* (2009) P02032.
- [44] O. Shpielberg and E. Akkermans, *Phys. Rev. Lett.* **116**, 240603 (2016).
- [45] O. Shpielberg, Y. Don, and E. Akkermans, *Phys. Rev. E* **95**, 032137 (2017).
- [46] L. Bertini, A. De Sole, D. Gabrielli, G. Jona-Lasinio, and C. Landim, *Phys. Rev. Lett.* **94**, 030601 (2005).
- [47] Y. Baek, Y. Kafri, and V. Lecomte, *Phys. Rev. Lett.* **118**, 030604 (2017).
- [48] A. Imparato, V. Lecomte, and F. van Wijland, *Phys. Rev. E* **80**, 011131 (2009).
- [49] J. Tailleur, J. Kurchan, and V. Lecomte, *Phys. Rev. Lett.* **99**, 150602 (2007).
- [50] A. N. Jordan, E. V. Sukhorukov, and S. Pilgram, *J. Math. Phys.* **45**, 4386 (2004).
- [51] P. C. Martin, E. Siggia, and H. Rose, *Phys. Rev. A* **8**, 423 (1973).
- [52] Notice that in this case, W is nonconvex. W must be convexified to obtain the proper solution, much like a free energy for thermodynamic phase transitions. See the full discussion in Ref. [46].
- [53] G. Gallavotti and E. G. D. Cohen, *Phys. Rev. Lett.* **74**, 2694 (1995).
- [54] B. Derrida, M. R. Evans, V. Hakim, and V. Pasquier, *J. Phys. A: Math. Gen.* **26**, 1493 (1993).
- [55] B. Derrida, B. Douçot, and P.-E. Roche, *J. Stat. Phys.* **115**, 717 (2004).
- [56] S. Katz, J. L. Lebowitz, and H. Spohn, *Phys. Rev. B* **28**, 1655(R) (1983).
- [57] S. Katz, J. L. Lebowitz, and H. Spohn, *J. Stat. Phys.* **34**, 497 (1984).
- [58] J. S. Hager, J. Krug, V. Popkov, and G. M. Schütz, *Phys. Rev. E* **63**, 056110 (2001).
- [59] T. Nemoto and S.-i. Sasa, *Phys. Rev. Lett.* **112**, 090602 (2014).
- [60] H. Spohn, Equilibrium fluctuations, in *Large Scale Dynamics of Interacting Particles*, Texts and Monographs in Physics (Springer, Berlin/Heidelberg, 1991), Part II, Chap. 2, pp. 175–211.